Proximity-dependent biotinylation and identification of flagellar proteins in *Trypanosoma cruzi*

Madalyn M. Won[1], Aaron Baublis[2], Barbara A. Burleigh[1]

[1]Department of Immunology and Infectious Diseases, Harvard T. H. Chan School of Public Health Boston, MA 02115, USA

[2]Harvard Chan Advanced Multi-omics Platform, Harvard T.H. Chan School of Public Health, Boston, Massachusetts 02115, USA

Corresponding Author: Barbara Burleigh: bburleig@hsph.harvard.edu

Running Title: Flagellar protein identification in *Trypanosoma cruzi*

Abstract

The flagellated kinetoplastid protozoan and causative agent of human Chagas disease, *Trypanosoma cruzi,* inhabits both invertebrate and mammalian hosts over the course of its complex life cycle. In these disparate environments, *T. cruzi* uses its single flagellum to propel motile life stages and in some instances, to establish intimate contact with the host. Beyond its role in motility, the functional capabilities of the *T. cruzi* flagellum have not been defined. Moreover, the lack of proteomic information for this organelle, in any parasite life stage, has limited functional investigation. In this study, we employed a proximity-dependent biotinylation approach based on the differential targeting of the biotin ligase, TurboID, to the flagellum or cytosol in replicative stages of *T. cruzi,* to identify flagellar-enriched proteins by mass spectrometry. Proteomic analysis of the resulting biotinylated protein fractions yielded 218 candidate flagellar proteins in *T. cruzi* epimastigotes (insect stage) and 99 proteins in intracellular amastigotes (mammalian stage). Forty of these flagellar-enriched proteins were common to both parasite life stages and included orthologs of known flagellar proteins in other trypanosomatid species, proteins specific to the *T. cruzi* lineage and hypothetical proteins. With the validation of flagellar localization for several of the identified candidates, our results demonstrate that TurboID-based proximity proteomics is an effective tool for probing subcellular compartments in *T. cruzi.* The proteomic datasets generated in this work offer a valuable resource to facilitate functional investigation of the understudied *T. cruzi* flagellum.

Importance

Trypanosoma cruzi is a protozoan parasite that causes Chagas disease, which contributes substantial morbidity and mortality in South and Central America. Throughout its life cycle, *T. cruzi* interacts with insect and mammalian hosts via its single flagellum, establishing intimate contact with host membranes. Currently, few flagellar proteins have been identified in *T. cruzi* that could provide insight into the mechanisms involved in mediating physical and biochemical interactions with the host. Here, we set out to identify flagellar proteins in the main replicative stages of *T. cruzi* using a proximity-labeling approach coupled with mass spectrometry. The >200 candidate flagellar proteins identified represent the first large scale identification of candidate flagellar proteins in *T. cruzi* with preliminary validation. These data offer new avenues to investigate the biology of *T. cruzi* - host interactions, a promising area for development of new strategies aimed at the control of this pathogen.

Introduction

Trypanosoma cruzi is the uniflagellate protozoan parasite that causes Chagas disease, a chronic disease with severe outcomes including cardiomyopathies and gastrointestinal motility disorders [1,2]. *T. cruzi* has a complex life cycle that involves both invertebrate and mammalian hosts, in which the parasite undergoes marked developmental changes and alternates between actively dividing ('epimastigote' or 'amastigote' forms in insect and mammalian hosts, respectively) and non-dividing 'trypomastigote' forms in both hosts (life cycle schematic; **Supplementary Fig. 1**). In mammals, infection is initiated by motile trypomastigotes that actively invade host cells before converting to the non-motile amastigote stage that replicates in the host

cytoplasm. Intracellular *T. cruzi* amastigotes begin to replicate ~24 hours post-infection (hpi) and undergo several rounds of cell division before converting back to trypomastigotes that eventually rupture the host cell membrane (between ~90-120 hpi) to allow dissemination of the parasite and infection of new tissue sites. Once *T. cruzi* infection is established in mammalian hosts, parasites typically persist at low levels for the life of the host, giving rise to chronic infections that can trigger inflammation and pathology.

In both insect and mammalian hosts, *T. cruzi* can establish intimate contact with host structures using its single flagellum [3–5]. In triatomine vectors, epimastigotes attach to the hindgut by forming a hemidesmosome-like structure between the distal part of the flagellum and host rectal epithelium [5]. This attachment prevents the parasites from being flushed from the insect and is important for promoting differentiation to the infectious metacyclic stage [5]. In mammalian host cells, cytosolically-localized *T. cruzi* amastigotes establish intermittent contact with host mitochondria using their short motile flagellum [3,6]. Unlike the motile trypomastigote and epimastigote stages of *T. cruzi,* that have elongated flagella (up to 15 µm in length [7]), replicative intracellular amastigotes have a truncated flagellum (~2.7 µm) that extends just beyond the opening of the flagellar pocket [6]. Also, *T. cruzi* amastigotes retain a 9+2 axonemal structure found in motile trypanosomatid life stages [8], but lack a paraflagellar rod, a unique lattice-like structure that runs parallel to the axoneme in these organisms [9], and which is associated with several functions including flagellar motility and signal transduction [10]. It has long been assumed that the minimal amastigote flagellum serves no function other than to provide a structural platform for flagellar outgrowth during differentiation to

85 motile life stages [11]. However, recent observations that the flagellum of intracellular *T.*
86 *cruzi* amastigotes undergoes low frequency aperiodic 'beating' inside mammalian host
87 cells [6] and makes physical contact with the host mitochondria [3,6], indicate that the
88 amastigote flagellum has a functional role within the host cell. The interaction between
89 the *T. cruzi* amastigote flagellum and host mitochondria is comparable to the intimate
90 contact observed between the flagellum of intracellular *Leishmania mexicana*
91 amastigotes and the host parasitophorous vacuole membrane [12]. In the case of
92 *Leishmania*, it has been postulated that the amastigote flagellum has a sensory role
93 and/or functions in the delivery of parasite material to the infected host cell [12,13]. It is
94 therefore reasonable to predict that the *T. cruzi* amastigote flagellum may have similar
95 role(s) in its interactions with the intracellular environment of the host cell.

96 In addition to critical roles in motility, eukaryotic flagella (i.e. cilia) and non-motile
97 cilia have emerged as important sensory organelles that are equipped with signal
98 transduction systems and second messengers such as cyclic AMP (cAMP) [14] and
99 calcium [15,16] that coordinate cellular responses to external stimuli. Functions beyond cell
100 locomotion have also been ascribed to the flagellum of motile trypanosomatid life stages
101 [11,13,17–19], where the best understood example of sensory integration in these organisms
102 is the role of flagellar receptor-type adenylate cyclases and cAMP-depending signaling
103 in pH taxis and social motility in the insect stage of *Trypanosoma brucei* [20–23]. In
104 *Leishmania*, flagellar aquaporin has been implicated in osmotaxis [24] in the insect stage,
105 and the flagellar membrane may be a critical site for glucose [25,26] and arginine [27]
106 sensing in these parasites. Indeed, in both *T. brucei* and *Leishmania*, near
107 comprehensive flagellar proteomes have been generated using shot-gun proteomics of

isolated flagella [28–30] or of detergent and high salt extracted fractions of the parasite, yielding axonemal and paraflagellar rod proteins [31]. Further, in *T. brucei*, specific domains of the flagellum have been partially mapped using proximity-dependent biotinylation including flagellar attachment zone proteins [32] and the flagellar tip [33], a specialized signaling domain.

By comparison, we have little knowledge of the molecular composition of the *T. cruzi* flagellum. Beyond a core axonemal proteome that is predicted based on conservation across trypanosomatid species and life stages [34], few flagellar proteins that have the potential to serve as a functional interface with the host environment have been identified in any *T. cruzi* life stage [9,35,36]. The best characterized is the flagellar calcium-binding protein (FCaBP), a dual-acylated, 24 kDa Ca^{2+}-sensing protein that tethers to the inner leaflet of the flagellar membrane [37]. FCaBP is expressed in all *T. cruzi* life stages and is conserved across other trypanosomatid species, but its precise role in the biology of these organisms is unknown beyond its role as a calcium binding protein [36,38,39]. Additionally, we have recently localized small myristoylated protein 1-1 (TcSMP1-1) to the flagellum in amastigotes [6], but the overall proteomic landscape of the *T. cruzi* flagellum remains largely uncharacterized.

In this study, we pursued a targeted, proximity-dependent biotinylation (BioID) approach to identify flagellar membrane and membrane-proximal flagellar proteins in the replicative stages of *T. cruzi.* We report the identification of 218 and 99 candidate flagellar proteins in *T. cruzi* epimastigotes and intracellular amastigote stages, respectively, many of which are conserved in other trypanosomatid species with evidence of flagellar localization. Approximately 20% of the candidate flagellar proteins

were found to be restricted to the *T. cruzi* lineage, including a hypothetical protein that we confirmed localizes to the flagellar tip in *T. cruzi* epimastigotes and intracellular amastigotes. The novel BioID dataset identified here provides a critical foundation for investigation of the *T. cruzi* flagellum and its role in mediating interactions with diverse host environments.

Results

Flagellar and cytosolically targeted TurboID retains activity in *T. cruzi*

To facilitate the identification of flagellar proteins in *T. cruzi* using a proximity-dependent biotinylation approach, we generated transgenic parasites that express the biotin ligase, TurboID [40] in the parasite flagellum, as an in-frame fusion with C-terminal FLAG-tagged *T. cruzi* small myristoylated protein 1-1 (TcSMP1-1) (**Fig. 1A,B;** SMP1-1-FLAG-TurboID; **'***F-Turbo'*). TcSMP1-1 was chosen as the endogenous 'bait' protein for flagellar localization of TurboID given its near exclusive localization in the flagellum in both replicative stages of *T. cruzi*, epimastigotes and amastigotes [6] (**Fig. 1A**), and because TcSMP1-1 contains the N-myristoylation sequence motif (MGXXXS/T) required for localization and tethering to the inner flagellar membrane, as demonstrated in *Leishmania* [41]. The strategy of targeting TurboID to the flagellum using TcSMP1-1 is expected to increase the likelihood of identifying flagellar membrane and associated proteins while minimizing capture of axonemal proteins. To control for non-flagellar TurboID expression in the F-Turbo parasites, we generated an independent transgenic line that expresses FLAG-TurboID in the cytoplasm (**Fig. 1B; '***C-Turbo'*). The parallel processing of F-Turbo and C-Turbo parasites, along with parental (WT) parasites that

lack TurboID expression (**Fig. 1C)**, will allow for background subtraction and identification of flagellar-enriched proteins in F-Turbo versus C-Turbo within the same parasite life cycle stage.

TurboID expression in transgenic *T. cruzi* parasites was confirmed by indirect immunofluorescence microscopy of fixed parasites stained with an antibody to the FLAG tag epitope, located immediately upstream of TurboID (**Fig. 2**). The flagella of F-Turbo parasites were brightly stained (**Fig. 2A,C;** *F-Turbo*) indicating that trafficking of TurboID to the flagellum occurred in both *T. cruzi* epimastigote (**Fig. 2A;** *F-Turbo*) and amastigote (**Fig. 2C;** *F-Turbo*) life stages. While most of the FLAG signal was localized to the flagellum in epimastigotes (**Fig. 2A;** *F-Turbo*), signal was detected in the body of intracellular amastigotes in addition to the brightly stained flagellum (**Fig. 2C;** *F-Turbo*), which may be due to overexpression of the SMP1-1-FLAG-TurboID fusion protein. C-Turbo parasites, generated as a proteomic control for non-flagellar TurboID-dependent biotinylation (**Fig. 1C**), were confirmed to express cytosolic FLAG in both parasite life stages (**Fig. 2A,C;** *C-Turbo***)**. To determine if TurboID is active in *T. cruzi*, total protein lysates were prepared from WT and Turbo-expressing parasites, following brief exposure to exogenous biotin, were probed with streptavidin-DyLight™ 800 to detect biotinylated proteins (**Fig. 2B,D**). As expected, multiple biotinylated proteins were revealed in lysates derived from F-TurboID and C-TurboID epimastigotes (**Fig. 2B**) and amastigotes (**Fig. 2D**) whereas few biotinylated proteins were detected in the parental (WT) controls. Differences in the biotinylated protein profiles observed when comparing F-Turbo to C-Turbo within a single life stage (**Fig. 2B,D)** likely reflect the differential localization patterns for TurboID in these parasite lines. Combined, these results

confirm the expression of active TurboID in the flagellum (F-Turbo) or cytosol (C-Turbo) in both replicative stages of *T. cruzi*.

Proteomic identification of candidate flagellar proteins in *T. cruzi*

Biotinylated proteins in lysates generated from WT, F-Turbo and C-Turbo *T. cruzi* epimastigotes or intracellular amastigotes, were captured on immobilized streptavidin beads and identified using high performance liquid chromatography combined with mass spectrometry (**Fig. 1C**). Three independent biological replicates were analyzed for each parasite line, with the exception of F-Turbo epimastigotes, for which triplicate samples from two independent transfections were included. Peptide identification and relative intensity data obtained for replicate samples from each parasite line are represented in **Supplementary Table 1**. Principal component analysis (PCA) identified overall trends in the proteomic data obtained for *T. cruzi* epimastigotes (**Fig. 3A**) and amastigotes (**Fig. 3C**), revealing that biological replicates from individual parasite lines (WT, F-Turbo, C-Turbo) formed discrete clusters that were well separated from each other. As the replicates from independent F-Turbo epimastigote lineages were indistinguishable, these samples were pooled for subsequent analyses. Prior to data filtering and analysis, protein intensity scores were averaged across biological replicates within individual experimental groups (**Supplementary Table 1**).

Streptavidin-bound proteins identified by mass spectrometry in WT parasites (which lack TurboID) represent the ‘background’ signal of endogenously biotinylated proteins and proteins that bound non-specifically to immobilized streptavidin. Thus, proteins represented at less than 100-fold enriched over the WT samples in F-Turbo or

C-Turbo epimastigote samples were removed before subsequent analysis. Also, any proteins identified in less than 4/6 of the F-Turbo samples were removed (**Supplementary Table 2**). Volcano plots revealed the protein subsets significantly enriched in F-Turbo and C-Turbo samples in epimastigotes (**Fig. 3B**) and amastigotes (**Fig. 3D**). Proteins found to be significantly enriched in F-Turbo over C-Turbo (fold-change > 2; q-value ≤ 0.01) as well as proteins identified uniquely in F-Turbo samples (i.e., not present in C-Turbo samples from the same parasite life stage) are listed in **Supplementary Table 3**. From this analysis, 218 proteins were identified as significantly enriched in F-Turbo samples from *T. cruzi* epimastigotes and 99 proteins in amastigotes (**Supplementary Table 3**).

The *T. cruzi* SMP1-1 proximity proteome includes known trypanosomatid flagellar proteins.

The searchable TrypTag database [42], which contains localization data for 7,487 *T. brucei* proteins, was used as a resource to identify orthologues in the *T. cruzi* flagellar-enriched protein dataset (**Supplementary Table 3**) that have demonstrated flagellar localization in *T. brucei*. Of the 218 flagellar-enriched proteins in *T. cruzi* epimastigotes, 145 have orthologs that are represented in the TrypTag database and of these, 75 proteins exhibit at least partial flagellar localization in *T. brucei* bloodstream forms [42]. Similar results emerged from the *T. cruzi* amastigote data where orthologs of 75 of the 99 proteins found to be enriched in amastigote F-Turbo samples had orthologs in *T. brucei* and were endogenously tagged, 44 of these showed at least partial flagellar localization. A comparison of the flagellar-enriched proteins identified in both *T. cruzi*

epimastigotes and amastigotes revealed 40 proteins common to both life stages (**Fig. 3E**), of which 29 have orthologs that are represented in the TrypTag database (**Supplementary Table 3**) and 20 proteins exhibited some flagellar localization in *T. brucei*. Examples of confirmed flagellar proteins in other trypanosomatids that are significantly enriched in the *T. cruzi* flagellar proximity proteome include: flagellar membrane 8 [43], flabarin [44], flagellar attachment zone 14 [32], casein kinase I [42], CARP3 [20] and cysteine peptidase, Clan CA, family C2 (calpain 1.3) [42]. Although a significant proportion of the flagellar candidates identified in *T. cruzi* epimastigotes and amastigotes fall into the 'hypothetical' category (i.e., no annotation), the datasets were found to be enriched in kinase domains, calpain domains, and small GTP binding protein / GTPase domains (**Fig. 3F**).

Selected flagellar candidates localize to the *T. cruzi* flagellum in epimastigotes and amastigotes.

To localize candidate flagellar proteins in *T. cruzi*, we prioritized those that were significantly enriched in both the epimastigote and amastigote F-Turbo datasets and that included one or more of the following characteristics: (a) sequence motifs predicting membrane localization; (b) predicted role in signaling based on annotation or (c) were unique to the *T. cruzi* lineage (i.e., no obvious orthologues in other trypanosomatid species). Based on these criteria, six proteins were selected for endogenous FLAG-tagging and subsequent subcellular localization (**Table 1**) using primers and homology-directed repair templates shown in (**Supplementary Fig. 4**). Four of the 6 proteins were successfully tagged and three of which exhibited flagellar localization in *T. cruzi*

epimastigotes: calpain 1.3 (TcCLB.506563.200), CARP3 (TcCLB.506681.40) and hypothetical protein (TcCLB.510329.180) (**Fig. 4A; Supplementary Fig. 2)**. Another hypothetical protein (TcCLB.509965.20) was not verified as flagellar as the FLAG epitope signal localized to the parasite body (data not shown). Calpain 1.3-mRuby2-smFP FLAG exhibited a punctate pattern of labeling along the entire length of the *T. cruzi* epimastigote flagellum (**Fig. 4A**), whereas expression appeared to be restricted to the flagellar tip in the intracellular amastigote stage (**Fig. 4B**). Both CARP3 and the hypothetical protein (TcCLB.510329.180) localized to the distal region of the epimastigote flagellum (**Fig. 4A**) and hypothetical protein (TcCLB.510329.180) also localized to the flagellar tip in amastigotes (**Fig. 4B**). We were unable to determine CARP3 localization in amastigotes, due to undetectable signal for CARP3-mRuby2-smFP FLAG expression in this life stage, despite clear signal and flagellar localization in epimastigotes (**Fig. 4A**). Nonetheless, the successful identification of a subset of flagellar-localized proteins in intracellular *T. cruzi* amastigotes and epimastigotes provides initial validation of the proteomic datasets generated from proximity-dependent labeling.

Discussion

In the present work we demonstrate the successful use of a proximity labeling tool in the protozoan parasite, *Trypanosoma cruzi.* With the goal of identifying flagellar membrane and/or associated proteins in *T. cruzi* as candidates for mediating physical or functional interactions with insect or vertebrate hosts, the biotin ligase TurboID was targeted to the parasite flagellum as a fusion protein with the inner flagellar membrane

protein, SMP1-1. Overexpression of the fusion protein was well-tolerated in the parasite, with no interference in the ability to transition between axenic epimastigotes, the *T. cruzi* life stage in which DNA transfection and selection is performed, and the intracellular stages in mammalian cells. This offered the opportunity to perform a comparative analysis of the two main replicative stages of *T. cruzi*, one that is motile with an elongated flagellum (epimastigote) and the other that is non-motile with a short flagellum (intracellular amastigote). Furthermore, inclusion of cytosolic-TurboID expressing parasites in the analysis aided in the differential identification of flagellar-enriched biotinylated proteins derived from SMP1-1-FLAG-TurboID parasites. This approach yielded 218 flagellar candidates in epimastigotes and 99 proteins in amastigotes, where 40 proteins were common to both *T. cruzi* life stages. Flagellar localization was confirmed for a subset of proteins in this dataset, based on endogenous epitope-tagging, and many more were predicted based on demonstrated localization in the related trypanosomatids, *T. brucei* or *Leishmania spp*.

The functional capabilities of the *T. cruzi* flagellum are broadly uncharacterized, beyond its role in propelling motile life stages and anchoring epimastigotes to the rectal mucosa in the insect vector [4,45,46]. However, the recent recognition that the flagellum of cytosolically-localized intracellular amastigotes is capable of beating and establishes physical contact with host mitochondria [3,6], points to a potential role for the amastigote flagellum in host environmental sensing. Although little is known regarding the sensory capabilities of trypanosomatids in general, significant progress has been made toward a molecular understanding of pH taxis and social motility in the insect stages of *T. brucei* [21,23]. The sensory system involves regulation of cyclic AMP levels, modulated by

292 flagellar receptor-type adenylate cyclases and cyclic AMP phosphodiesterases[22] and
293 the involvement of a cyclic AMP responsive protein (CARP3), which is thought to act in
294 a complex with adenylate cyclases [20]. Our discovery, that CARP3 is expressed in the
295 replicative stages of *T. cruzi,* including intracellular amastigotes (despite the inability to
296 localize the tagged protein in this life stage), is quite exciting given the established role
297 of CARP3 in *T. brucei* [20]*.* In *T. brucei* CARP3 is known to co-localize with calpain 1.3 at
298 the distal region of the flagellum, where the two proteins may physically interact [20]. We
299 show that the calpain 1.3 ortholog is also expressed in the flagellum of *T. cruzi,* where it
300 localizes exclusively to the flagellar tip in intracellular amastigotes, a recognized
301 signaling domain in trypanosomatids [33(p2),47]. Calpain 1.3 belongs to a sub-family of
302 cysteine peptidases that are predicted to be catalytically inactive as they lack one or
303 more of the active site amino acid residues [48]. Proteins with these features are thought
304 to play a role in calcium homeostasis / signaling, including the calcium-based regulation
305 of adenylate cyclase complexes [20,49]. Despite the lack of social motility in *T. cruzi,* the
306 expression of flagellar CARP3 and calpain 1.3 in this species is a strong indicator that
307 the *T. cruzi* flagellum is equipped to sense and integrate signals from the environment.
308 Dissection of the functional roles of CARP3 and calpain 1.3 in *T. cruzi* is expected to be
309 instrumental in establishing the existence of flagellum-based environmental sensing in
310 this parasite. In addition, a functional investigation of the hypothetical protein
311 (TcCLB.509965.20) that also localizes to the distal end of the *T. cruzi* flagellum but
312 lacks an obvious ortholog in *T. brucei* or *Leishmania*, has the potential to reveal novel
313 biological or mechanistic insights into the role of the *T. cruzi* flagellum in different life
314 stages.

The proteomic datasets generated here offer new opportunities to pursue the localization and functional analyses of many uncharacterized proteins, some of which are unique to the *T. cruzi* lineage. While some of the annotated proteins are not predicted to localize to the flagellum (based on annotation and TrypTag localization), including proteins involved in protein trafficking which may have encountered SMP1-1-FLAG-TurboID *en route* to the flagellum, there are a number of proteins with transmembrane domains or N-myristoylation consensus sequences that predict membrane-association. SMP-1 contains the N-myristoylation sequence motif (MGXXXS/T) known to direct flagellar localization and tethering to the inner flagellar membrane in *Leishmania*, where it associates tightly with detergent-resistant membranes (lipid rafts) [41] and forms homodimers [41]. As such, SMP1-1 may preferentially interact with other membrane proteins associated with lipid rafts in the flagellar membrane. It is notable that a number of proteins that were among the strongest 'hits' in the flagellar candidate pool, such as calpain 1.3 and CARP3, also have MGXXXS/T motifs. While this motif is insufficient to direct a protein to the flagellum [41], proteins with lipid anchoring motifs or transmembrane domains could be prioritized for future studies of the *T. cruzi* flagellum. Notably, we did not identify adenylate cyclases in our data, even though CARP3 and calpain 1.3 were identified in a proximity-labeling study in *T. brucei* designed to identify flagellar tip proteins that interact with adenylate cyclase 1 [33]. While the proximity-dependent labeling approach used in this study enabled the discovery of a subset of flagellar proteins in *T. cruzi* amastigotes (where physical isolation of the short amastigote flagellum may not be feasible), it is understood that the resulting proteomes derived for the two parasite life stages are not

338 comprehensive and many *T. cruzi* flagellar membrane proteins remain to be identified.
339 With the discovery of additional flagellar proteins in *T. cruzi,* opportunities will be
340 presented to use one or more of these proteins as alternative bait proteins for proximity
341 labeling with a view to expanding the flagellar proteome in this understudied parasite.

342 Overall, we have presented the first use of proximity-dependent biotinylation in *T.*
343 *cruzi* for the identification of more than 200 candidate flagellar proteins across two
344 parasite life stages, thereby creating an important resource for the research community.
345 As more information becomes available for the *T. cruzi* amastigote flagellum, it is
346 expected to provide some context for the biological role of the flagellum in infection and
347 these interactions may be the key for specific targeting of parasite function and viability
348 within the mammalian host. Future investigation focused on identifying the function of
349 potential sensory flagellar candidates in *T. cruzi* epimastigote and amastigote flagella,
350 may aid in the discovery of these currently unknown host-parasite interaction
351 mechanisms.

352

353 **Methods and Materials**

354 **Reagents**

355 Compounds were purchased and diluted to stock concentrations: Biotin, 100 mM in
356 DMSO (Sigma Aldrich, St. Louis, Missouri, USA). Phenylmethylsulfonyl fluoride (PMSF),
357 10 mM in isopropanol (Sigma Aldrich, St. Louis, Missouri, USA). Tosyl-L-lysyl-
358 chloromethane hydrochloride (TLCK), 5 mM in DMSO (Abcam, Cambridge, United
359 Kingdom).

360

Mammalian cell culture

Normal Human Neonatal Dermal Fibroblasts (NHDF; Lonza, Basel, Switzerland) and monkey kidney epithelial cells (LLC-MK2; American Type Culture Collection) were maintained in Dulbecco's modified Eagle medium (DMEM; HyClone, Logan, Utah, USA) supplemented with 10% heat-inactivated FBS (Gibco, Waltham, Massachusetts, USA), 25 mM glucose, 2 mM L-glutamine, and 100 U/mL penicillin-streptomycin (DMEM-10) at 37°C and 5% CO_2.

Growth and maintenance of *T. cruzi*

Trypanosoma cruzi Tulahuén LacZ clone C4 was obtained from the American Type Culture Collection (ATCC, PRA-330; ATCC, Manassas, Virginia, USA). The epimastigote stage was propagated at 28°C in liver infusion tryptose (LIT) medium (4□g/L NaCl, 0.4□g/L KCl, 8□g/L Na2HPO4, 2□g/L dextrose, 3□g/L liver infusion broth, 5□g/L tryptose, with 25□mg/L hemin and 10% heat-inactivated FBS). The mammalian cell infection cycle was initiated with metacyclic trypomastigotes arising within stationary phase epimastigote cultures that were shifted from LIT to DMEM + 2% FBS (DMEM-2) for 5 days at 28°C. Metacyclic-enriched cultures were washed in DMEM-2 and incubated with confluent LLC-MK2 monolayers at 37°C, 5% CO_2 to allow invasion. Mammalian stage trypomastigotes that emerged from infected LLC-MK2 cells (within 5-10 days) were harvested from culture supernatants and used to infect fresh LLC-MK2 monolayers. This cycle was continued on weekly basis to maintain the mammalian-infective stages of *T. cruzi* in culture. For experimental infections, trypomastigotes collected from LLC-MK2 maintenance cultures were pelleted at 2060 x g for 10 minutes

and pellets were incubated at 37°C, 5% CO_2 for 2-4 hours to allow motile trypomastigotes to swim up into the supernatant. Purified trypomastigotes in the supernatant were collected, washed once in DMEM-2 and utilized to infect sub-confluent monolayers of NHDF as indicated.

Generation of stable *T. cruzi* transfectants

T. cruzi strains expressing TcSMP1-1GFP were previously generated [6]. A plasmid containing the TurboID sequence was a kind gift of Jeffrey Dvorin (Harvard Medical School). Each TurboID construct was used to replace the GFP-P2A-puro cassette in a modified pTREX plasmid [50,51] containing either SMP1-1-GFP or GFP alone. The inserts in the pTREX backbone to generate the F-Turbo plasmids were SMP1-1-TurboID-P2A-puro (F-Turbo-P) or SMP-1-1-TurboID-T2A-puro (F-Turbo-T). The inserts and backbone were assembled using the NEB HiFi DNA assembly kit (New England Biolabs, Ipswich, Massachusetts, USA), resulting in the final plasmids. For the cytosolic control, TurboID-P2A-puro was amplified using PCR and then inserted into the pTREX-GFP backbone, replacing GFP between the SpeI and XmaI cut sites using or through restriction enzyme cloning. To generate TurboID-expressing parasites *T. cruzi* epimastigotes were transfected with 15 µg of the respective DNA. Prior to transfection log-phase *T. cruzi* epimastigotes, were pelleted at 2060 x g for 10 minutes, resuspended in 100 µL of Tb BSF buffer [52] ($4x10^7$ parasites) and placed into a sterile 2 mm gap cuvette with the appropriate DNA and transfected using an Amaxa Nucleofector II (Lonza, Basel, Switzerland; U-33 program). Parasites were immediately transferred to LIT medium for

24 hours before adding 10 µg/mL puromycin (Invivogen, San Diego, California, USA) or 50 µg/mL blasticidin (Invivogen, San Diego, California, USA) for selection.

CRISPR/Cas9-facilitated epitope tagging of genomic loci in *T. cruzi* was performed as described [53]. Briefly, each gene of interest was PCR-amplified from genomic DNA (*T. cruzi* Tulahuen strain) and PCR products sequenced. Two gRNA binding sites near the 3' region of each gene of interest were identified using EuPaGDT [54]. Editing of the previously modified pTREX-n-Cas9 plasmid [51] (Addgene plasmid 68708), performed to exchange the previous gRNA sequence was achieved using a Q5 mutagenesis kit (New England Biolabs, Ipswich, Massachusetts, USA). gRNA sequences were inserted into pTREX-n-Cas9 using primers specific to the gene of interest in **Supplementary Table 4**, such that the previous gRNA sequence was replaced. The template for generating homology-directed repair DNA for gene tagging was constructed by inserting a P2A viral skip peptide in frame with a downstream blasticidin-S deaminase (BSD) or puromycin N-acetyl-transferase (puro) and TOPO cloned into a pCR4 backbone (Thermo Fisher, Waltham, MA, United States of America) [51]. Homology template was amplified from this template using ultramer pairs (**Supplementary Table 4**) that provided 100 bp of homology for the gene of interest, the FLAG tag and 20 bp of homology to template. Parasite were transfected as above with 25 µg of each gRNA-specific pTREX-n-Cas9 plasmid to the gene of interest and 50 µg of homology repair template. Correct integration of the endogenous tag and drug cassette was established via PCR (**Supplementary Fig. 2**).

Detection of biotinylated protein fractions in *T. cruzi*

Epimastigotes: 1.5 x 10^8 epimastigotes were pelleted at 2060 x g for 10 minutes, resuspended in 1 ml of LIT and incubated with 50 µM biotin for 10 minutes at 37^{o}C. Parasites were washed twice with ice-cold PBS then resuspended in 1 ml cell lysis buffer [55] (0.5% Nonidet P-40, 500 mM NaCl, 5 mM EDTA, 1 mM DTT, 50 mM Tris-Base, 0.4% SDS, pH 7.4) with Roche cOmplete™ Protease Inhibitor (Sigma-Aldrich, St. Louis, Missouri, USA), 100 µM PMSF and 10 µM TLCK. Lysates were sonicated using 3 pulses of 30 seconds at 100% amplitude (Q700 sonicator, QSONICA, Newton, Connecticut), with 15 sec breaks between to cool the tubes on ice. Samples were centrifuged at 16,000 x g for 20 minutes at 4°C and the supernatant was collected. Aliquots of clarified lysate (3 x 10^6 parasite equivalents) were resolved by SDS-PAGE (Mini-PROTEAN®TGX protein gel; Bio-Rad, Hercules, California, USA), transferred to PVDF membrane (Immobilon®-FL, MilliporeSigma, Burlington, Massachusetts, USA) and probed with Streptavidin DyLight™ 800 (Thermo Fisher Scientific, Waltham, Massachusetts, USA) to detect biotinylated proteins.

Intracellular amastigotes: At 48 hpi, *T. cruzi*-infected NHDF monolayers in T-150 flasks were exposed to 100 µM biotin for 10 minutes at 37°C, 5% CO_2. Monolayers were then rinsed three times with cold PBS and incubated with 2 mL of cell lysis buffer (as above). Flasks were agitated manually for 5 minutes then cells were scraped and transferred into a tube containing 0.5 µL of benzonase (Sigma-Aldrich, St. Louis, Missouri, USA). Tubes were placed on a rotative wheel for 15 minutes at room temperature, then sonicated as above. Amastigote loading volumes were normalized via Western blot as

follows. Equal volumes of serially diluted protein lysates, generated for WT, F-Turbo and C-Turbo infected NHDF, were resolved by SDS-PAGE (Mini-PROTEAN®TGX gels), transferred to PVDF membrane and probed with a rabbit antibody to trypanosome BiP [56], followed by α-Rabbit Alexa Flour 647. A LiCor Odessy® CLx imager was used to measure BiP signal in each sample (Image Studio). Relative BiP densities were used to adjust the volumes of each amastigote lysates (confirmed by independent western blots) prior to loading on streptavidin beads.

Isolation of biotinylated proteins

Protein lysates were loaded onto Pierce™ High-Capacity Streptavidin Agarose (Thermo Fisher Scientific, Waltham, Massachusetts, USA). 100 µL and 150 µL packed bead volumes were used for epimastigote and amastigote samples, respectively, and incubated on a rotative wheel overnight at 4°C. For all following steps, washes consisted of adding 1 mL of the indicated buffer and placing the tube on the rotative wheel for 5 minutes, then spinning down the agarose beads for 1 minute at 500 x g, as previously described [55]. Beads with bound protein were subjected to 5 washes with Buffer 1 (8 M urea, 200 mM NaCl, 100 mM Tris, pH 8.0) with 0.2% sodium dodecyl sulfate (SDS), 5 washes with Buffer 1 containing 2% SDS, and 5 washes with Buffer 1 with no SDS were completed at room temperature. Next, 2 washes with 200 mM NaCl, 100 mM Tris, at a pH of 7.0 and 2 washes with Tris, pH 8.0 were completed at 4°C. Washed beads were adjusted to pH 7.5 with 200 mM HEPES (4-(2-hydroxyethyl)-1-piperazineethanesulfonic acid) and bound proteins were reduced using 5 mM dithiothreitol (Sigma-Aldrich) at 37°C for 1 h, followed by alkylation of cysteine residues

using 15 mM iodoacetamide (Sigma-Aldrich) in the dark at room temperature for 1 h. Excessive iodoacetamide was quenched using 10 mM dithiotheritol. Protein mixtures were diluted in 1:6 ratio (v/v) using ultrapure water prior to digestion using sequencing grade trypsin (Promega) at 37°C for 16 h. Digested peptides were subsequently desalted using self-packed C18 STAGE tips (3M EmporeTM) [57] for LC-MS/MS analysis.

Mass spectrometry

Epimastigotes: Desalted peptides were resuspended in 0.1% (v/v) formic acid and loaded onto HPLC-MS/MS system for analysis on an Orbitrap Q-Exactive Exploris 480 (Thermo Fisher Scientific) mass spectrometer coupled to an Easy nanoLC 1000 (Thermo Fisher Scientific) with a flow rate of 250 nl/min. The stationary phase buffer was 0.5 % formic acid and mobile phase buffer was 0.5 % (v/v) formic acid in acetonitrile. Chromatography for peptide separation was performed using increasing organic proportion of acetonitrile (5 – 40 % (v/v)) over a 120 min gradient) on a self-packed analytical column using PicoTipTM emitter (New Objective, Woburn, MA) using Reprosil Gold 120 C-18, 1.9 µm particle size resin (Dr. Maisch, Ammerbuch-Entringen, Germany). The mass spectrometry analyzer operated in data dependent acquisition mode with a top ten method at a mass range of 300–2000 Da. Data were processed using MaxQuant software (version 1.5.2.8) [58] with the following setting: oxidized methionine residues and protein N-terminal acetylation as variable modification, cysteine carbamidomethylation as fixed modification, first search peptide tolerance 20 ppm, main search peptide tolerance 4.5 ppm. Protease specificity was set to trypsin

498 with up to 2 missed cleavages allowed. Only peptides longer than five amino acids were
499 analyzed, and the minimal ratio count to quantify a protein is 2 (proteome only). The
500 false discovery rate (FDR) was set to 1% for peptide and protein identifications.
501 Database searches were performed using the Andromeda search engine integrated into
502 the MaxQuant environment [59] against the UniProt *Trypanosoma cruzi* strain CL Brener
503 (352153) database containing 19,242 entries (March 2020). “Matching between runs”
504 algorithm with a time window of 0.7 min was employed to transfer identifications
505 between samples processed using the same nanospray conditions. Protein tables were
506 filtered to eliminate identifications from the reverse database and common
507 contaminants.
508
509 *Amastigotes*: Desalted peptides were resolubilized in 0.1% (v/v) formic acid and loaded
510 onto HPLC-MS/MS system for analysis on an Orbitrap Q-Exactive Exploris 480 (Thermo
511 Fisher Scientific) mass spectrometer coupled to an FAIMS Pro Interface system and
512 Easy nanoLC 1000 (Thermo Fisher Scientific) with a flow rate of 300 nl/min. The
513 stationary phase buffer was 0.1 % formic acid, and mobile phase buffer was 0.1 % (v/v)
514 formic acid in 80% (v/v) acetonitrile. Chromatography for peptide separation was
515 performed using increasing organic proportion of acetonitrile (5 – 40 % (v/v)) over a 120
516 min gradient) on a self-packed analytical column using PicoTip™ emitter (New
517 Objective, Woburn, MA) using Reprosil Gold 120 C-18, 1.9 µm particle size resin (Dr.
518 Maisch, Ammerbuch-Entringen, Germany). High precision iRT calibration was used for
519 samples processed using the same nanospray conditions [60]. The mass spectrometry
520 analyzer operated in data independent acquisition mode at a mass range of 300–

2000 Da, compensation voltages of -50/-70 CVs with survey scan of 120,000 and 15,000 resolutions at MS1 and MS2 levels, respectively. Data were processed using Spectronaut™ software (version 15; Biognosys AG) [61] using directDIA™ analysis with default settings, including: oxidized methionine residues, biotinylation, protein N-terminal acetylation as variable modification, cysteine carbamidomethylation as fixed modification, initial mass tolerance of MS1 and MS2 of 15 ppm. Protease specificity was set to trypsin with up to 2 missed cleavages were allowed. Only peptides longer than seven amino acids were analyzed, and the minimal ratio count to quantify a protein is 2 (proteome only). The false discovery rate (FDR) was set to 1% for peptide and protein identifications. Database searches were performed against the UniProt *Trypanosoma cruzi* strain CL Brener (352153) database containing 19,242 entries (March 2020). Protein tables were filtered to eliminate identifications from the reverse database and common contaminants.

Principal component analysis

All protein intensity scores were uploaded to Metaboanalyst 5.0 [62] to perform statistical analysis, with one factor. Data was entered as peak intensities and filtered using the interquartile range, then normalized by sum and log transformed. 2D PCA scores were plotted in Prism GraphPad.

Volcano plots

For epimastigote data, protein intensity scores for all proteins that were found to be 100-fold or higher enriched in the F-Turbo or C-Turbo samples over wild type were loaded

into Prism GraphPad, and Log_{10} transformed. Multiple unpaired t-tests were run on the data with a false discovery rate of 1% and the results were reported as F-Turbo – C-Turbo, with -log10(q value) reported for the volcano plot. For amastigote data, Spectronaut™ software was used to generate the statistical analysis of the amastigote proteomics. Within the DIA analysis pipeline, the default settings were used, including a false discovery rate of 1% and a n unpaired Student's t-test was performed. Fold changes were reported as an average Log10 (epimastigotes) or Log2 (amastigotes) ratio for the volcano plot. Volcano plot was created in Prism GraphPad. Post-analysis, six proteins were excluded from the amastigote flagellar enriched list, as they were not identified in 2 of 3 biological replicates. Additionally, all allelic duplicates were removed to ensure that the proteins listed in the final tables were represented by a single gene identifier corresponding to the CL Brener reference genome (TriTrypDB; https://tritrypdb.org/), but paralogs remain.

Interpro domain enrichment analysis

DAVID [63] enrichment was used to assign Interpro domains to all of the proteins found to be significantly enriched in either of the F-Turbo samples. No weighting of the data was completed. Interpro domains with a p-value ≤ 0.05 were considered significantly enriched.

Indirect immunofluorescence microscopy

Epimastigotes were fixed directly in growth medium with the addition of paraformaldehyde (1% final concentration in PBS) for 10-minute at 4°C. Fixed parasites

were pelleted by centrifuging for 10 minutes at 4000 x g and resuspended in PBS. 10 µL of the parasite solution was dropped onto poly-L-lysine coated slides and allowed to dry completely prior to staining. For immunostaining of intracellular amastigotes, *T. cruzi*-infected NHDF on round cover glass (12 mm, #1.5; Electron Microscopy Sciences, Hatfield, Pennsylvania, USA) were fixed at 48 hours post-infection with 1% (v/v) paraformaldehyde/PBS. All steps of the immunostaining protocol were preceded by three washes with PBS and carried out at room temperature. Parasites were permeabilized with a 0.1% Triton-X 100 solution (JT Baker, Phillipsburg, New Jersey, USA) for 10 minutes and blocked with 3% BSA (Sigma-Aldrich, St. Louis, Missouri, USA) in PBS for 1 hour. The primary antibody solution containing 1:400 mouse α-FLAG (clone M2, Sigma-Aldrich, St. Louis, Missouri, USA) and/or 1:1,500 rabbit α-FCaBP [64] in 1% BSA in PBS was added for 1 hour, followed by a 1:1000 α-Mouse Alexa Flour 594 and/or α-Rabbit Alexa Flour 647 solution in 1% BSA in PBS for 1 hour. DAPI (0.2 µg/mL; Thermo Fisher Scientific, Waltham, Massachusetts, USA) in PBS was added for 5 minutes, and following washes, coverslips were placed onto slides with Prolong® Diamond mountant (Thermo Fisher Scientific, Waltham, Massachusetts, USA). After setting for 24 hours parasites were imaged using a Yokogawa CSU-X1 spinning disk confocal system paired with a Nikon Ti-E inverted microscope and an iXon Ultra 888 EMCCD camera (100X objective). Image processing, analysis, and display were performed using ImageJ Fiji software [65].

Acknowledgments

We thank the Sabri Ülker Center's Advanced Imaging Lab at the Harvard T.H. Chan School of Public Health for microscopy training and access. Additionally, we would like to thank Zon Weng Lai from the Harvard Chan Advanced Multi-omics Platform at the Harvard T.H. Chan School of Public Health for his assistance in interpreting the mass spectrometry data. We thank Jeffrey Dvorin (Boston Children's Hospital) for providing the TurboID plasmid, David Engman (Cedars-Sinai Medical Center) for the gift of the anti-FCaBP antibody and Jay Bangs (The State University of New York at Buffalo) for anti-BiP antibody. We also thank Lucas Pagura for his thoughtful discussion. This work was supported by NIH grant R21AI135520 awarded to BAB and NIH training grant 5T32AI049928.

Competing interests

No competing interests declared.

Table 1: Candidate flagellar proteins in *T. cruzi* selected for endogenous tagging**.**

Name	TriTryp ID	Successfully Tagged?	Reason for selection
Calpain 1.3	TcCLB.506563.200	Yes	Potential signaling role
CARP3	TcCLB.506681.40	Yes	Potential signaling role
Hypothetical Protein	TcCLB.510329.180	Yes	No known ortholog
Hypothetical Protein	TcCLB.509965.20	Yes	No known *T. brucei* ortholog
ATPase	TcCLB.506925.410	No	Potential transmembrane protein
Hypothetical Protein	TcCLB.509011.50	No	Potential signaling role

Candidates from the 40 proteins identified in both *T. cruzi* epimastigotes and amastigotes selected for endogenous epitope tagging and localization.

606

607

608 **References**

609 1. Bern C. Chagas' Disease. *N Engl J Med*. 2015;373(5):456-466.
610 doi:10.1056/NEJMra1410150

611 2. Stanaway JD, Roth G. The burden of Chagas disease: estimates and challenges.
612 *Glob Heart*. 2015;10(3):139-144. doi:10.1016/j.gheart.2015.06.001

613 3. Lentini G, Dos Santos Pacheco N, Burleigh BA. Targeting host mitochondria: A role
614 for the *Trypanosoma cruzi* amastigote flagellum. *Cell Microbiol*. 2018;20(2).
615 doi:10.1111/cmi.12807

616 4. Nogueira NFS, Gonzalez MS, Gomes JE, de Souza W, Garcia ES, Azambuja P,
617 Nohara LL, Almeida IC, Zingales B, Colli W. *Trypanosoma cruzi*: involvement of
618 glycoinositolphospholipids in the attachment to the luminal midgut surface of
619 Rhodnius prolixus. *Exp Parasitol*. 2007;116(2):120-128.
620 doi:10.1016/j.exppara.2006.12.014

621 5. Schmidt J, Kleffmann T, Schaub GA. Hydrophobic attachment of *Trypanosoma cruzi*
622 to a superficial layer of the rectal cuticle in the bug *Triatoma infestans*. *Parasitol*
623 *Res*. 1998;84(7):527-536. doi:10.1007/s004360050443

624 6. Won MM, Krüger T, Engstler M, Burleigh BA. The intracellular amastigote of
625 *Trypanosoma cruzi* maintains an actively beating flagellum. *mBio*. In Press.

626 7. Gonçalves CS, Ávila AR, de Souza W, Motta MCM, Cavalcanti DP. Revisiting the
627 *Trypanosoma cruzi* metacyclogenesis: morphological and ultrastructural analyses
628 during cell differentiation. *Parasit Vectors*. 2018;11:83. doi:10.1186/s13071-018-
629 2664-4

630 8. Gadelha C, Wickstead B, McKean PG, Gull K. Basal body and flagellum mutants
631 reveal a rotational constraint of the central pair microtubules in the axonemes of
632 trypanosomes. *J Cell Sci*. 2006;119(Pt 12):2405-2413. doi:10.1242/jcs.02969

633 9. Gardiner PJ. Pellicle-associated structures in the amastigote stage of *Trypanosoma*
634 *cruzi* and *Leishmania* species. *Ann Trop Med Parasitol*. 1974;68(2):167-176.
635 doi:10.1080/00034983.1974.11686935

636 10. Portman N, Gull K. The paraflagellar rod of kinetoplastid parasites: From structure
637 to components and function. *Int J Parasitol*. 2010;40(2):135.
638 doi:10.1016/j.ijpara.2009.10.005

639 11. Kelly FD, Sanchez MA, Landfear SM. Touching the Surface: Diverse Roles for the
640 Flagellar Membrane in Kinetoplastid Parasites. *Microbiol Mol Biol Rev MMBR*.
641 2020;84(2):e00079-19. doi:10.1128/MMBR.00079-19

642 12. Gluenz E, Höög JL, Smith AE, Dawe HR, Shaw MK, Gull K. Beyond 9+0:
643 noncanonical axoneme structures characterize sensory cilia from protists to

644 humans. *FASEB J Off Publ Fed Am Soc Exp Biol*. 2010;24(9):3117-3121.
645 doi:10.1096/fj.09-151381

646 13. Kelly FD, Yates PA, Landfear SM. Nutrient Sensing in *Leishmania*: Flagellum and
647 Cytosol. *Mol Microbiol*. Published online October 28, 2020. doi:10.1111/mmi.14635

648 14. Saegusa Y, Yoshimura K. cAMP controls the balance of the propulsive forces
649 generated by the two flagella of *Chlamydomonas*. *Cytoskelet Hoboken NJ*.
650 2015;72(8):412-421. doi:10.1002/cm.21235

651 15. Bickerton P, Sello S, Brownlee C, Pittman JK, Wheeler GL. Spatial and temporal
652 specificity of Ca2+ signalling in *Chlamydomonas reinhardtii* in response to osmotic
653 stress. *New Phytol*. 2016;212(4):920-933. doi:10.1111/nph.14128

654 16. Christensen ST, Pedersen LB, Schneider L, Satir P. Sensory cilia and integration of
655 signal transduction in human health and disease. *Traffic*. 2007;8(2):97-109.
656 doi:10.1111/j.1600-0854.2006.00516.x

657 17. Camara M de los M, Bouvier LA, Miranda MR, Pereira CA. The flagellar adenylate
658 kinases of *Trypanosoma cruzi*. *FEMS Microbiol Lett*. 2015;362(1):1-5.
659 doi:10.1093/femsle/fnu020

660 18. Langousis G, Hill KL. Motility and more: the flagellum of *Trypanosoma brucei*. *Nat*
661 *Rev Microbiol*. 2014;12(7):505-518. doi:10.1038/nrmicro3274

662 19. Peacock L, Bailey M, Carrington M, Gibson W. Meiosis and haploid gametes in the
663 pathogen *Trypanosoma brucei*. *Curr Biol CB*. 2014;24(2):181-186.
664 doi:10.1016/j.cub.2013.11.044

665 20. Bachmaier S, Giacomelli G, Calvo-Alvarez E, Vieira LR, Abbeele JVD,
666 Aristodemou A, Lorentzen E, Gould M, Brennand A, Dupuy JW, Forné I, imhof A,
667 Bramkamp M, Salmon D, Rotureau B, Boshart M. A multi-adenylate cyclase
668 regulator at the flagellar tip controls African trypanosome transmission. Published
669 online 2022. doi:10.21203/rs.3.rs-1216579/v1

670 21. Shaw S, Knüsel S, Abbühl D, Naguleswaran A, Etzensperger R, Benninger M,
671 Roditi I. Cyclic AMP signalling and glucose metabolism mediate pH taxis by African
672 trypanosomes. *Nat Commun*. 2022;13(1):603. doi:10.1038/s41467-022-28293-w

673 22. Oberholzer M, Saada EA, Hill KL. Cyclic AMP Regulates Social Behavior in African
674 Trypanosomes. *mBio*. 2015;6(3):e01954-14. doi:10.1128/mBio.01954-14

675 23. Lopez MA, Saada EA, Hill KL. Insect stage-specific adenylate cyclases regulate
676 social motility in African trypanosomes. *Eukaryot Cell*. 2015;14(1):104-112.
677 doi:10.1128/EC.00217-14

678 24. Figarella K, Uzcategui NL, Zhou Y, LeFurgey A, Ouellette M, Bhattacharjee H,
679 Mukhopadhyay R. Biochemical characterization of *Leishmania major*

aquaglyceroporin LmAQP1: possible role in volume regulation and osmotaxis. *Mol Microbiol*. 2007;65(4):1006-1017. doi:10.1111/j.1365-2958.2007.05845.x

25. Rodriguez-Contreras D, Aslan H, Feng X, Tran K, Yates PA, Kamhawi S, Landfear SM. Regulation and biological function of a flagellar glucose transporter in *Leishmania mexicana*: a potential glucose sensor. *FASEB J Off Publ Fed Am Soc Exp Biol*. 2015;29(1):11-24. doi:10.1096/fj.14-251991

26. Piper RC, Xu X, Russell DG, Little BM, Landfear SM. Differential targeting of two glucose transporters from *Leishmania enriettii* is mediated by an NH2-terminal domain. *J Cell Biol*. 1995;128(4):499-508. doi:10.1083/jcb.128.4.499

27. Goldman-Pinkovich A, Kannan S, Nitzan-Koren R, Puri M, Pawar H, Bar-Avraham Y, McDonald J, Sur A, Zhang WW, Matlashewski G, Madhubala R, Michaeli S, Myler PJ, Zilberstein D. Sensing Host Arginine Is Essential for *Leishmania* Parasites' Intracellular Development. *mBio*. 2020;11(5). doi:10.1128/mBio.02023-20

28. Oberholzer M, Langousis G, Nguyen HT, Saada EA, Shimogawa MM, Jonsson ZO, Nguyen SM, Wohlschlegel JA, Hill KL. Independent Analysis of the Flagellum Surface and Matrix Proteomes Provides Insight into Flagellum Signaling in Mammalian-infectious *Trypanosoma brucei*. *Mol Cell Proteomics MCP*. 2011;10(10):M111.010538. doi:10.1074/mcp.M111.010538

29. Beneke T, Demay F, Hookway E, Ashman N, Jeffery H, Smith J, Valli J, Becvar T, Myskova J, Lestinova T, Shafiq S, Sadlova J, Volf P, Wheeler RJ, Gluenz E. Genetic dissection of a *Leishmania* flagellar proteome demonstrates requirement for directional motility in sand fly infections. *PLOS Pathog*. 2019;15(6):e1007828. doi:10.1371/journal.ppat.1007828

30. Subota I, Julkowska D, Vincensini L, Reeg N, Buisson J, Blisnick T, Huet D, Perrot S, Santi-Rocca J, Duchateau M, Hourdel V, Rousselle JC, Cayet N, Namane A, Chamot-Rooke J, Bastin P. Proteomic analysis of intact flagella of procyclic *Trypanosoma brucei* cells identifies novel flagellar proteins with unique sub-localization and dynamics. *Mol Cell Proteomics MCP*. 2014;13(7):1769-1786. doi:10.1074/mcp.M113.033357

31. Broadhead R, Dawe HR, Farr H, Griffiths S, Hart SR, Portman N, Shaw MK, Ginger ML, Gaskell SJ, McKean PG, Gull K. Flagellar motility is required for the viability of the bloodstream trypanosome. *Nature*. 2006;440(7081):224-227. doi:10.1038/nature04541

32. Hu H, Zhou Q, Li Z. SAS-4 Protein in *Trypanosoma brucei* Controls Life Cycle Transitions by Modulating the Length of the Flagellum Attachment Zone Filament. *J Biol Chem*. 2015;290(51):30453-30463. doi:10.1074/jbc.M115.694109

33. Vélez-Ramírez DE, Shimogawa MM, Ray SS, Lopez A, Rayatpisheh S, Langousis G, Gallagher-Jones M, Dean S, Wohlschlegel JA, Hill KL. APEX2 Proximity

Proteomics Resolves Flagellum Subdomains and Identifies Flagellum Tip-Specific Proteins in *Trypanosoma brucei*. *mSphere*. 2021;6(1):e01090-20. doi:10.1128/mSphere.01090-20

34. Branche C, Kohl L, Toutirais G, Buisson J, Cosson J, Bastin P. Conserved and specific functions of axoneme components in trypanosome motility. *J Cell Sci*. 2006;119(16):3443-3455. doi:10.1242/jcs.03078

35. Jimenez V, Docampo R. Molecular and Electrophysiological Characterization of a Novel Cation Channel of *Trypanosoma cruzi*. *PLOS Pathog*. 2012;8(6):e1002750. doi:10.1371/journal.ppat.1002750

36. Engman DM, Krause KH, Blumin JH, Kim KS, Kirchhoff LV, Donelson JE. A novel flagellar Ca2+-binding protein in trypanosomes. *J Biol Chem*. 1989;264(31):18627-18631.

37. Maric D, McGwire BS, Buchanan KT, Olson CL, Emmer BT, Epting CL, Engman DM. Molecular Determinants of Ciliary Membrane Localization of *Trypanosoma cruzi* Flagellar Calcium-binding Protein. *J Biol Chem*. 2011;286(38):33109-33117. doi:10.1074/jbc.M111.240895

38. Buchanan KT, Ames JB, Asfaw SH, Wingard JN, Olson CL, Campana PT, Araújo APU, Engman DM. A flagellum-specific calcium sensor. *J Biol Chem*. 2005;280(48):40104-40111. doi:10.1074/jbc.M505777200

39. Maldonado RA, Mirzoeva S, Godsel LM, Lukas TJ, Goldenberg S, Watterson DM, Engman DM. Identification of calcium binding sites in the trypanosome flagellar calcium-acyl switch protein. *Mol Biochem Parasitol*. 1999;101(1-2):61-70. doi:10.1016/s0166-6851(99)00055-9

40. Branon TC, Bosch JA, Sanchez AD, Udeshi ND, Svinkina T, Carr SA, Feldman JL, Perrimon N, Ting AY. Efficient proximity labeling in living cells and organisms with TurboID. *Nat Biotechnol*. 2018;36(9):880-887. doi:10.1038/nbt.4201

41. Tull D, Naderer T, Spurck T, Mertens HDT, Heng J, McFadden GI, Gooley PR, McConville MJ. Membrane protein SMP-1 is required for normal flagellum function in *Leishmania*. *J Cell Sci*. 2010;123(Pt 4):544-554. doi:10.1242/jcs.059097

42. Dean S, Sunter JD, Wheeler RJ. TrypTag.org: A Trypanosome Genome-wide Protein Localisation Resource. *Trends Parasitol*. 2017;33(2):80-82. doi:10.1016/j.pt.2016.10.009

43. Calvo-Álvarez E, Bonnefoy S, Salles A, Benson FE, McKean PG, Bastin P, Rotureau B. Redistribution of FLAgellar Member 8 during the trypanosome life cycle: Consequences for cell fate prediction. *Cell Microbiol*. 2021;23(9):e13347. doi:10.1111/cmi.13347

44. Tetaud E, Lefebvre M, M'Bang-Benet DE, Crobu L, Blancard C, Sterkers Y, Pages M, Bastien P, Merlin G. TbFlabarin, a flagellar protein of *Trypanosoma brucei*, highlights differences between *Leishmania* and *Trypanosoma* flagellar-targeting signals. *Exp Parasitol*. 2016;166:97-107. doi:10.1016/j.exppara.2016.04.004

45. Kollien A, Schaub G. The Development of *Trypanosoma cruzi* in Triatominae. *Parasitol Today*. 2000;16(9):381-387. doi:10.1016/S0169-4758(00)01724-5

46. Cámara M de los M, Balouz V, Centeno Cameán C, Cori CR, Kashiwagi GA, Gil SA, Macchiaverna NP, Cardinal MV, Guaimas F, Lobo MM, de Lederkremer RM, Gallo-Rodriguez C, Buscaglia CA. *Trypanosoma cruzi* surface mucins are involved in the attachment to the *Triatoma infestans* rectal ampoule. *PLoS Negl Trop Dis*. 2019;13(5):e0007418. doi:10.1371/journal.pntd.0007418

47. Varga V, Moreira-Leite F, Portman N, Gull K. Protein diversity in discrete structures at the distal tip of the trypanosome flagellum. *Proc Natl Acad Sci U S A*. 2017;114(32):E6546-E6555. doi:10.1073/pnas.1703553114

48. Rawlings ND, Barrett AJ. Families of cysteine peptidases. In: *Methods in Enzymology*. Vol 244. Proteolytic Enzymes: Serine and Cysteine Peptidases. Academic Press; 1994:461-486. doi:10.1016/0076-6879(94)44034-4

49. Liu W, Apagyi K, McLeavy L, Ersfeld K. Expression and cellular localisation of calpain-like proteins in *Trypanosoma brucei*. *Mol Biochem Parasitol*. 2010;169(1):20-26. doi:10.1016/j.molbiopara.2009.09.004

50. DaRocha WD, Silva RA, Bartholomeu DC, Pires SF, Freitas JM, Macedo AM, Vazquez MP, Levin MJ, Teixeira SMR. Expression of exogenous genes in *Trypanosoma cruzi*: improving vectors and electroporation protocols. *Parasitol Res*. 2004;92(2):113-120. doi:10.1007/s00436-003-1004-5

51. Dumoulin PC, Vollrath J, Won MM, Wang JX, Burleigh BA. Endogenous Sterol Synthesis Is Dispensable for *Trypanosoma cruzi* Epimastigote Growth but Not Stress Tolerance. *Front Microbiol*. 2022;13:937910. doi:10.3389/fmicb.2022.937910

52. Schumann Burkard G, Jutzi P, Roditi I. Genome-wide RNAi screens in bloodstream form trypanosomes identify drug transporters. *Mol Biochem Parasitol*. 2011;175(1):91-94. doi:10.1016/j.molbiopara.2010.09.002

53. Lander N, Chiurillo MA, Vercesi AE, Docampo R. Endogenous C-terminal Tagging by CRISPR/Cas9 in *Trypanosoma cruzi*. *Bio-Protoc*. 2017;7(10). doi:10.21769/BioProtoc.2299

54. Tarleton R, Peng D. EuPaGDT: a web tool tailored to design CRISPR guide RNAs for eukaryotic pathogens. *Microb Genomics*. 2015;1(4). doi:10.1099/mgen.0.000033

55. Kelly FD, Tran KD, Hatfield J, Schmidt K, Sanchez MA, Landfear SM. A Cytoskeletal Protein Complex is Essential for Division of Intracellular Amastigotes of *Leishmania mexicana*. *bioRxiv*. Published online April 30, 2020:2020.04.29.068445. doi:10.1101/2020.04.29.068445

56. Bangs JD, Uyetake L, Brickman MJ, Balber AE, Boothroyd JC. Molecular cloning and cellular localization of a BiP homologue in *Trypanosoma brucei*. Divergent ER retention signals in a lower eukaryote. *J Cell Sci*. 1993;105 (Pt 4):1101-1113.

57. Rappsilber J, Ishihama Y, Mann M. Stop and go extraction tips for matrix-assisted laser desorption/ionization, nanoelectrospray, and LC/MS sample pretreatment in proteomics. *Anal Chem*. 2003;75(3):663-670. doi:10.1021/ac026117i

58. Cox J, Mann M. MaxQuant enables high peptide identification rates, individualized p.p.b.-range mass accuracies and proteome-wide protein quantification. *Nat Biotechnol*. 2008;26(12):1367-1372. doi:10.1038/nbt.1511

59. Cox J, Neuhauser N, Michalski A, Scheltema RA, Olsen JV, Mann M. Andromeda: a peptide search engine integrated into the MaxQuant environment. *J Proteome Res*. 2011;10(4):1794-1805. doi:10.1021/pr101065j

60. Bruderer R, Bernhardt OM, Gandhi T, Reiter L. High-precision iRT prediction in the targeted analysis of data-independent acquisition and its impact on identification and quantitation. *Proteomics*. 2016;16(15-16):2246-2256. doi:10.1002/pmic.201500488

61. Bruderer R, Bernhardt OM, Gandhi T, Miladinović SM, Cheng LY, Messner S, Ehrenberger T, Zanotelli V, Butscheid Y, Escher C, Vitek O, Rinner O, Reiter L. Extending the limits of quantitative proteome profiling with data-independent acquisition and application to acetaminophen-treated three-dimensional liver microtissues. *Mol Cell Proteomics MCP*. 2015;14(5):1400-1410. doi:10.1074/mcp.M114.044305

62. Pang Z, Zhou G, Ewald J, Chang L, Hacariz O, Basu N, Xia J. Using MetaboAnalyst 5.0 for LC-HRMS spectra processing, multi-omics integration and covariate adjustment of global metabolomics data. *Nat Protoc*. 2022;17(8):1735-1761. doi:10.1038/s41596-022-00710-w

63. Sherman BT, Hao M, Qiu J, Jiao X, Baseler MW, Lane HC, Imamichi T, Chang W. DAVID: a web server for functional enrichment analysis and functional annotation of gene lists (2021 update). *Nucleic Acids Res*. Published online March 23, 2022:gkac194. doi:10.1093/nar/gkac194

64. Maric D, Olson CL, Xu X, Ames JB, Engman DM. Calcium-dependent membrane association of a flagellar calcium sensor does not require calcium binding. *Mol Biochem Parasitol*. 2015;201(1):72-75. doi:10.1016/j.molbiopara.2015.06.003

829 65. Schindelin J, Arganda-Carreras I, Frise E, Kaynig V, Longair M, Pietzsch T,
830 Preibisch S, Rueden C, Saalfeld S, Schmid B, Tinevez JY, White DJ, Hartenstein
831 V, Eliceiri K, Tomancak P, Cardona A. Fiji: an open-source platform for biological-
832 image analysis. *Nat Methods*. 2012;9(7):676-682. doi:10.1038/nmeth.2019

833

834

Figure Legends

Figure 1. *T. cruzi* life cycle and schematic of TurboID-expressing lines generated for proximity-dependent biotinylation experiments. (**A**) Live confocal images of SMP1-1-GFP localized to the flagellum of *T. cruzi* epimastigotes and an intracellular amastigote; white oval denotes position of amastigote body. (**B**) Strategy for generating stable *T. cruzi* lines expressing TurboID in the flagellum using SMP1-1 as the endogenous bait protein or in the cytoplasm of epimastigotes and amastigotes, where addition of exogenous biotin will mediate biotinylation (red star) of proteins in close proximity to TurboID in both settings. FLAG-epitope is included to facilitate TurboID localization in transfectants. (**C**) Flow chart outlining the experimental protocol used for identification of biotinylated proteins in epimastigotes (*left*) and intracellular amastigotes (*right*). For both life stages, wild-type *('WT'*), cytoplasmic-TurboID ('*C'*) and flagellar-TurboID ('*F'*) parasites (from left to right in the illustration) were exposed to biotin and the biotinylated protein fraction in protein lysates captured on streptavidin-agarose beads and subjected to mass spectrometry for identification and subsequent proteomic analysis.

Figure 2. TurboID localization and activity in *T. cruzi*. (**A,C**) Fluorescence microscopy images of fixed *T. cruzi* epimastigotes (**A**) or amastigotes (**C**) expressing SMP1-1-FLAG-TurboID (F-Turbo) (*top*) or FLAG-TurboID (C-Turbo) (*bottom*) stained for FLAG epitope (anti-FLAG)(*pink*). In (**C**), white arrows indicate the position of the amastigote flagellum. (**B,D**) Biotinylated proteins in lysates of WT, F-Turbo, and C-

858 Turbo *T. cruzi* epimastigote (**B**) and amastigotes (**D**) detected with streptavidin-
859 Dylight800.
860
861 **Figure 3. Proximity proteome analysis identifies flagellar-enriched proteins in *T.***
862 ***cruzi*.** Principal component analysis (PCA) of biotinylome data plotted for WT (*no*
863 *TurboID control*), flagellar-TurboID (*F-Turbo*) and cytosolic-TurboID (*C-Turbo*) for *T.*
864 *cruzi* epimastigotes (**A**) and intracellular amastigotes (**C**). The two independent F-Turbo
865 groups in the epimastigote PCA plot are represented in green (triangles and squares).
866 Volcano plots (**B,D**) with fold-change (F-Turbo vs C-Turbo; x-axis) and adjusted p-value
867 (q-value; y-axis) for *T. cruzi* epimastigote (**B**) and amastigote (**D**) proteomic data.
868 Horizontal lines represent a q-value of 0.01 and the two vertical lines indicate the cut-
869 offs for fold change (2-fold). The top right quadrants in each plot (**B,D**) contain proteins
870 that are significantly enriched in F-Turbo proteomes ($q \leq 0.01$, $\geq$2-fold change). Known
871 trypanosomatid flagellar proteins (*purple circles)* and hypothetical proteins *(green*
872 *circles*) are shown for the F-Turbo enriched proteins. (**E**) Venn diagram depicting the
873 number of proteins identified as enriched in the F-Turbo samples of *T. cruzi*
874 epimastigote and amastigote stages. **(F**) Interpro domains assigned by DAVID that are
875 significantly enriched in F-Turbo samples (i.e. proteins found in the upper right quadrant
876 of each volcano plot) in epimastigotes, amastigotes and those common to both life
877 stages; *p*-value is a modified Fisher exact, for protein enrichment analysis.
878
879 **Figure 4. Flagellar localization of candidate flagellar proteins in *T. cruzi*.**
880 Endogenous tagging reveals flagellar localization of candidate flagellar proteins: calpain

1.3-smFLAG (TcCLB.506563.200), CARP3-smFLAG (TcCLB.506681.40), or hypothetical protein-FLAG (TcCLB.510329.180) in *T. cruzi* epimastigotes (**A**) or intracellular amastigotes (**B).** In all cases, the FLAG tag was detected in fixed parasites using an anti-FLAG antibody and secondary antibody (*green*) and the flagellum was detected using anti-FCaBP and secondary antibody (*magenta*). The FLAG signal in the flagellum is indicated (*yellow arrow*).

Supplementary Figure 1. Model of the *T. cruzi* life cycle. Schematic of the *T. cruzi* life cycle highlighting the insect stage '*epimastigote*' that is propagated axenically in liquid culture and gives rise to the infectious '*metacyclic trypomastigote*'. Trypomastigotes, whether derived from epimastigotes or as the end product of a single lytic cycle in a mammalian cell are motile, non-dividing forms of the parasite that actively invade a mammalian host cell. Inside a host cell, the '*trypomastigote'* transforms into the replicative intracellular '*amastigote'* stage by 18 hours post-infection (hpi). Amastigotes undergo several rounds of proliferation, dividing by binary fission (between ~24-90 hpi), before they stop dividing and differentiate into trypomastigotes, that eventually lyse the infected host cell and disseminate infection. Stable transfection and drug selection is performed in the epimastigote stage (lightning bolt symbolizes electroporation). Once stable genomic changes are confirmed in epimastigotes, these parasites are used to establish the mammalian infection cycle starting with metacyclic trypomastigotes as outlined above.

903 **Supplementary Figure 2: PCR confirmation of endogenous tags for candidate**
904 **proteins. A.** Schematic showing the region of amplification and DNA gel with
905 corresponding bands for **A**. calpain 1.3-smFLAG (TcCLB.506563.200), **B.** CARP3-
906 smFLAG (TcCLB.506681.40), and **C.** hypothetical protein-FLAG (TcCLB.510329.180).
907 Ladder run on all DNA gels is Thermo Scientific GeneRuler DNA Ladder.
908
909 **Supplementary Table 1: Raw proteomics data for epimastigotes and intracellular**
910 **amastigotes TurboID experiment.** Each sheet contains the protein identity and
911 intensity score for all samples in either epimastigotes or amastigotes.
912
913 **Supplementary Table 2: Filtered proteomics data for epimastigotes and**
914 **intracellular amastigotes TurboID experiment.** Each sheet contains the protein
915 identity and intensity score for all samples in either epimastigotes or amastigotes that
916 was used for statistical analysis.
917
918 **Supplementary Table 3: Proteins enriched in the flagellar TurboID expressing**
919 **samples for epimastigotes and intracellular amastigotes**. Each sheet contains
920 information about the proteins enriched in either epimastigotes, amastigotes, or both
921 epimastigotes and amastigotes.
922
923 **Supplementary Table 4: Primers for all PCR and endogenous tagging**. Primer pairs
924 are listed for all experiments described.
925

Figure 1: Won et al.

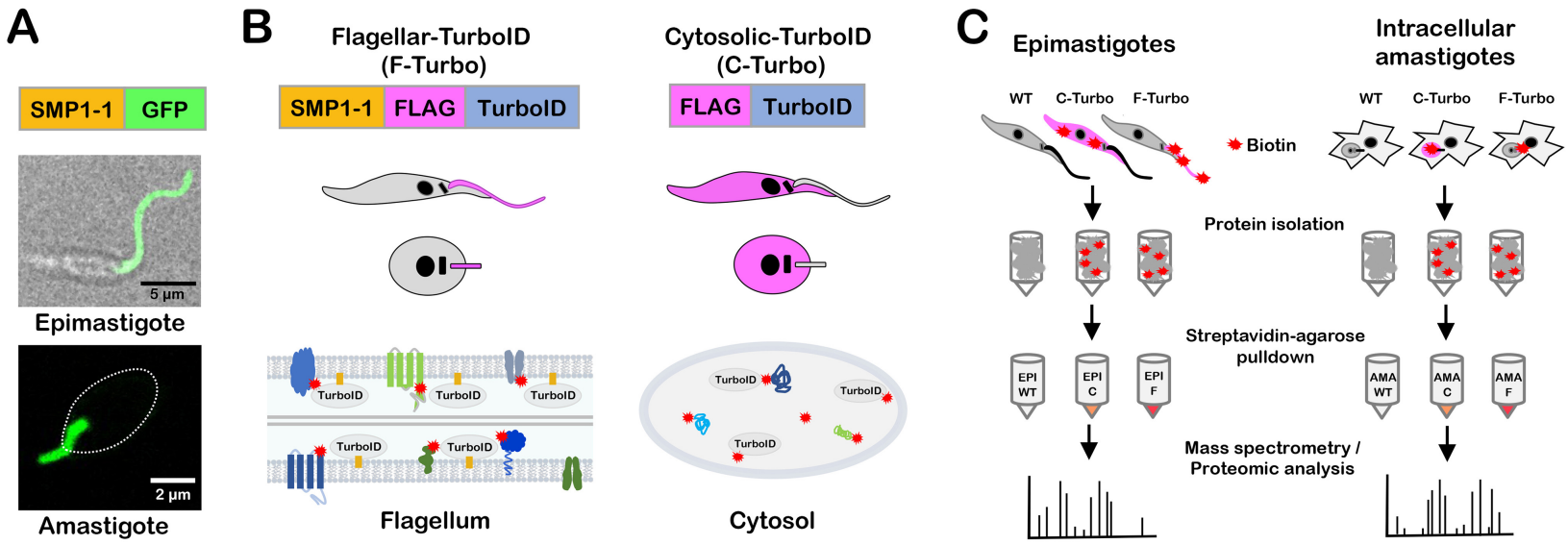

Figure 1. *T. cruzi* life cycle and schematic of TurboID-expressing lines generated for proximity-dependent biotinylation experiments. (**A**) Live confocal images of SMP1-1-GFP localized to the flagellum of *T. cruzi* epimastigotes and an intracellular amastigote; white oval denotes position of amastigote body. (**B**) Strategy for generating stable *T. cruzi* lines expressing TurboID in the flagellum using SMP1-1 as the endogenous bait protein or in the cytoplasm of epimastigotes and amastigotes, where addition of exogenous biotin will mediate biotinylation (red star) of proteins in close proximity to TurboID in both settings. FLAG-epitope is included to facilitate TurboID localization in transfectants. (**C**) Flow chart outlining the experimental protocol used for identification of biotinylated proteins in epimastigotes (*left*) and intracellular amastigotes (*right*). For both life stages, wild-type *('WT')*, cytoplasmic-TurboID ('*C*') and flagellar-TurboID ('*F*') parasites (from left to right in the illustration) were exposed to biotin and the biotinylated protein fraction in protein lysates captured on streptavidin-agarose beads and subjected to mass spectrometry for identification and subsequent proteomic analysis.

Figure 2: Won et al.

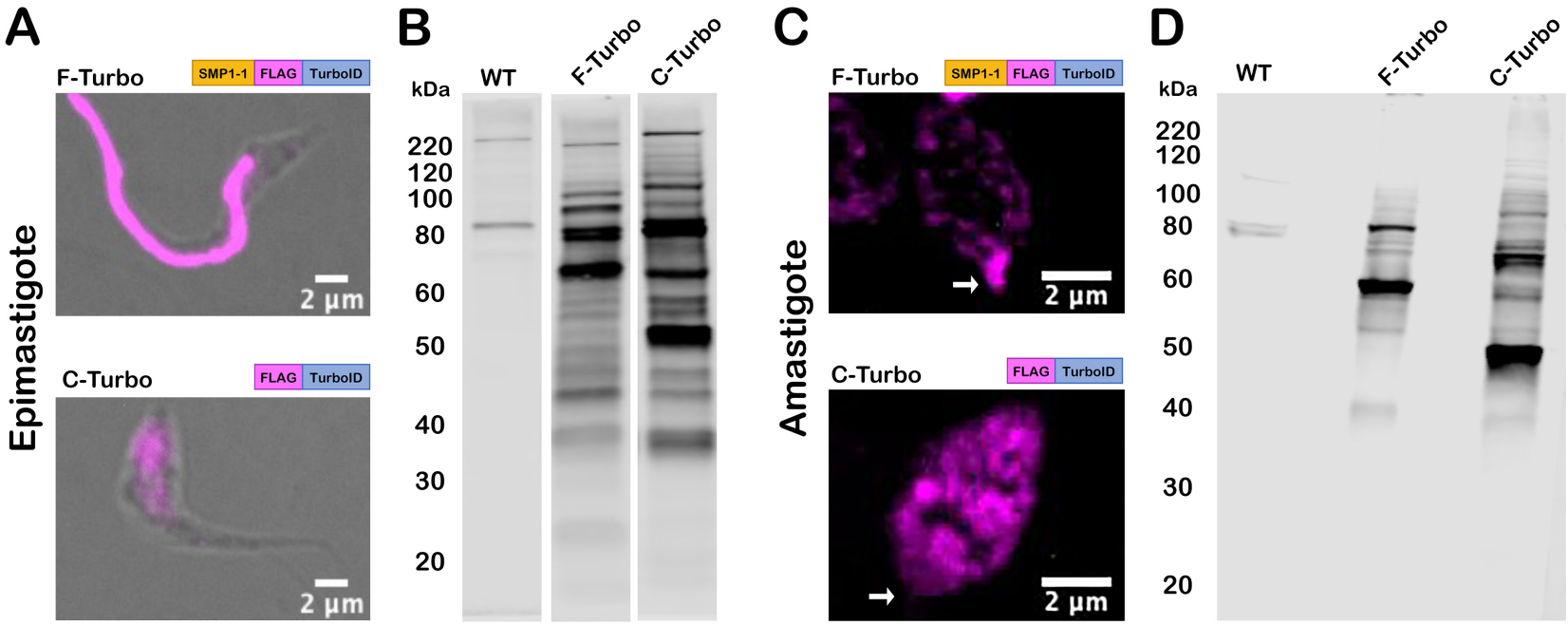

Figure 2. TurboID localization and activity in *T. cruzi*. (**A,C**) Fluorescence microscopy images of fixed *T. cruzi* epimastigotes (**A**) or amastigotes (**C**) expressing SMP1-1-FLAG-TurboID (F-Turbo) (*top*) or FLAG-TurboID (C-Turbo) (*bottom*) stained for FLAG epitope (anti-FLAG)(*pink*). In (**C**), white arrows indicate the position of the amastigote flagellum. (**B,D**) Biotinylated proteins in lysates of WT, F-Turbo, and C-Turbo *T. cruzi* epimastigote (**B**) and amastigotes (**D**) detected with streptavidin-Dylight800.

Figure 3: Won et al.

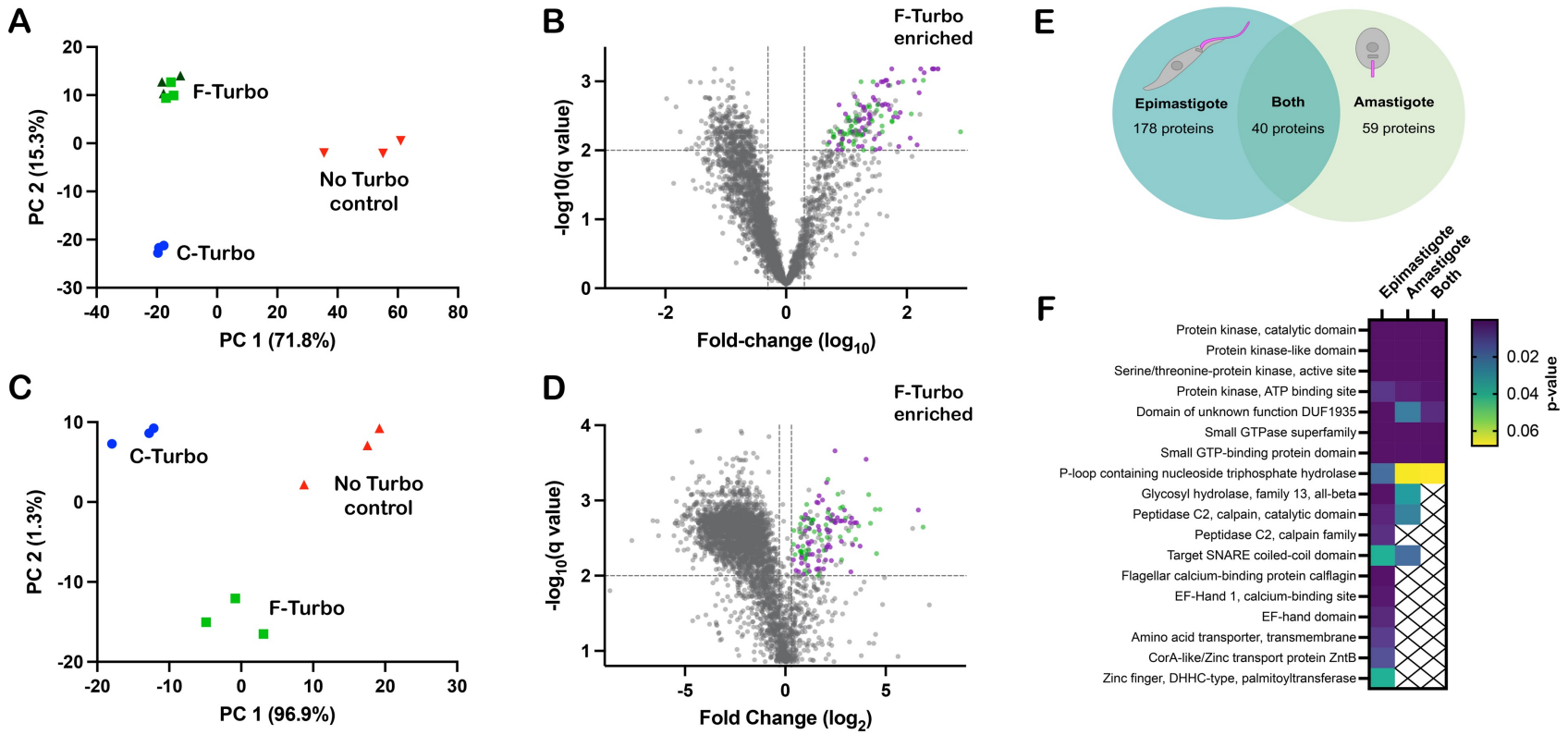

Figure 3. Proximity proteome analysis identifies flagellar-enriched proteins in *T. cruzi*. Principal component analysis (PCA) of biotinylome data plotted for WT (*no TurboID control*), flagellar-TurboID (*F-Turbo*) and cytosolic-TurboID (*C-Turbo*) for *T. cruzi* epimastigotes (**A**) and intracellular amastigotes (**C**). The two independent F-Turbo groups in the epimastigote PCA plot are represented in green (triangles and squares). Volcano plots (**B,D**) with fold-change (F-Turbo vs C-Turbo; x-axis) and adjusted p-value (q-value; y-axis) for *T. cruzi* epimastigote (**B**) and amastigote (**D**) proteomic data. Horizontal lines represent a q-value of 0.01 and the two vertical lines indicate the cut-offs for fold change (2-fold). The top right quadrants in each plot (**B,D**) contain proteins that are significantly enriched in F-Turbo proteomes ($q \leq 0.01$, $\geq$2-fold change). Known trypanosomatid flagellar proteins (*purple circles)* and hypothetical proteins *(green circles*) are shown for the F-Turbo enriched proteins. (**E**) Venn diagram depicting the number of proteins identified as enriched in the F-Turbo samples of *T. cruzi* epimastigote and amastigote stages. **(F)** Interpro domains assigned by DAVID that are significantly enriched in F-Turbo samples (i.e. proteins found in the upper right quadrant of each volcano plot) in epimastigotes, amastigotes and those common to both life stages; *p*-value is a modified Fisher exact, for protein enrichment analysis.

Figure 4: Won et al.

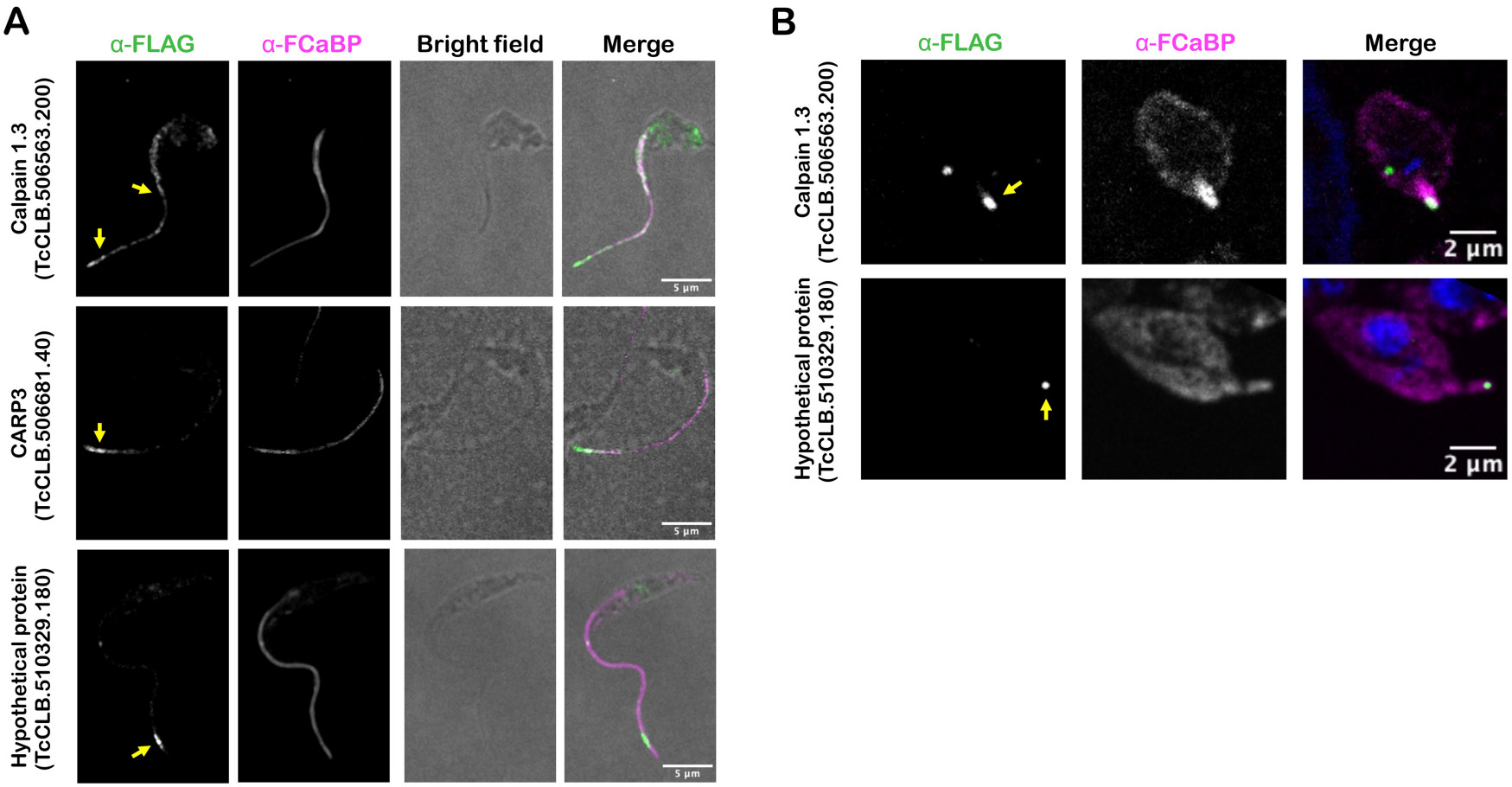

Figure 4. Flagellar localization of candidate flagellar proteins in *T. cruzi*. Endogenous tagging reveals flagellar localization of candidate flagellar proteins: calpain 1.3-smFLAG (TcCLB.506563.200), CARP3-smFLAG (TcCLB.506681.40), or hypothetical protein-FLAG (TcCLB.510329.180) in *T. cruzi* epimastigotes (**A**) or intracellular amastigotes (**B**)**.** In all cases, the FLAG tag was detected in fixed parasites using an anti-FLAG antibody and secondary antibody (*green*) and the flagellum was detected using anti-FCaBP and secondary antibody (*magenta*). The FLAG signal in the flagellum is indicated (*yellow arrow*).

Supplemental Figure 1: Won et al.

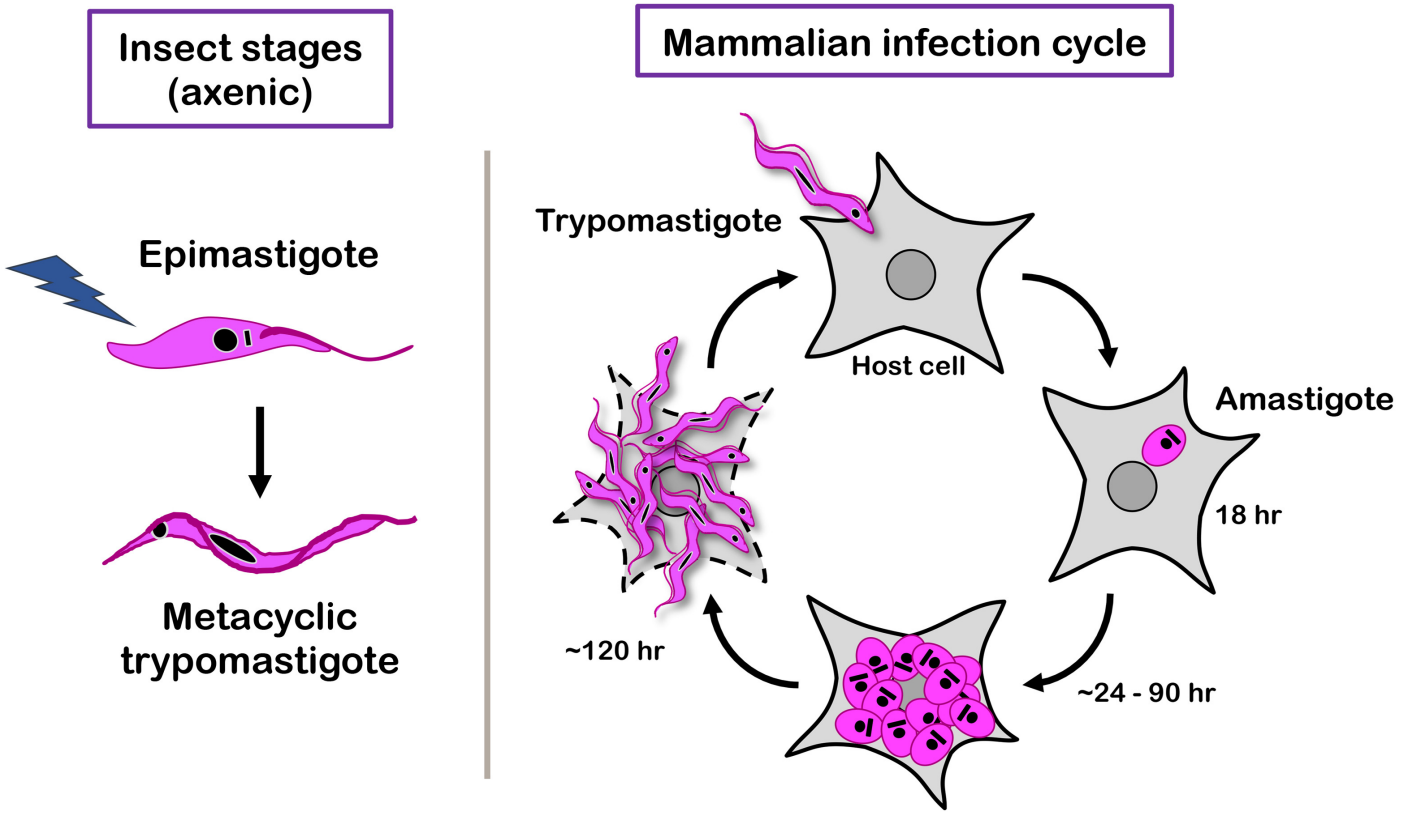

Supplemental Figure 1. **Schematic of the *T. cruzi* life cycle**. Insect stage '*epimastigote*' that is propagated axenically in liquid culture and gives rise to the infectious '*metacyclic trypomastigote*'. Trypomastigotes, whether derived from epimastigotes or as the end product of a single lytic cycle in a mammalian cell are motile, non-dividing forms of the parasite that actively invade a mammalian host cell. Inside a host cell, the '*trypomastigote'* transforms into the replicative intracellular '*amastigote'* stage by 18 hours post-infection (hpi). Amastigotes undergo several rounds of proliferation, dividing by binary fission (between ~24-90 hpi), before they stop dividing and differentiate into trypomastigotes, that eventually lyepimastigotese the infected host cell and disseminate infection. Stable transfection and drug selection is performed in the stage (lightning bolt symbolizes electroporation). Once stable genomic changes are confirmed in epimastigotes, these parasites are used to establish the mammalian infection cycle starting with metacyclic trypomastigotes as outlined above.

Supplemental Figure 2: Won et al.

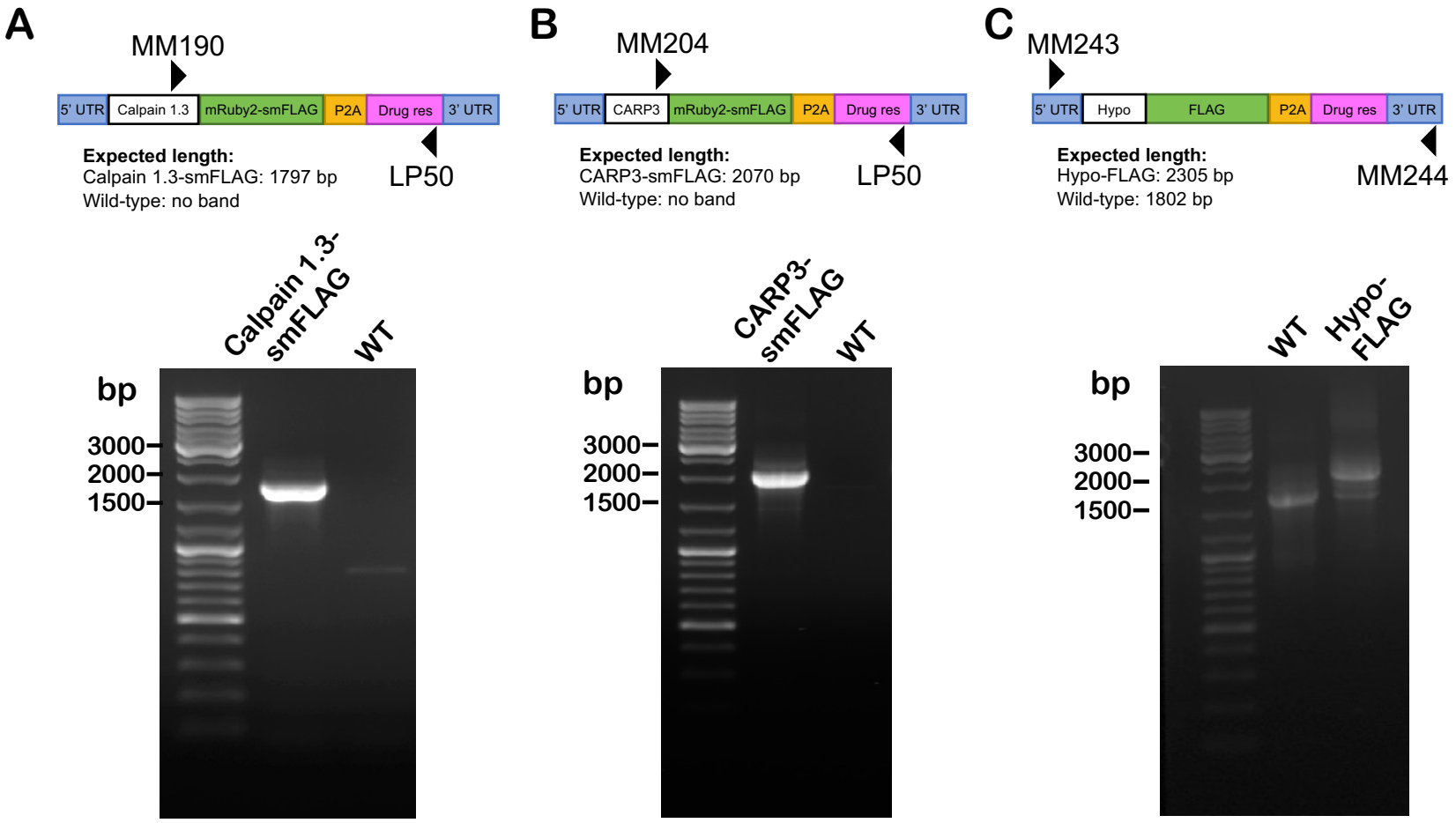

Supplemental Figure 2: PCR confirmation of endogenous tags for candidate proteins. A. Schematic showing the region of amplification and DNA gel with corresponding bands for **A**. calpain 1.3-smFLAG (TcCLB.506563.200), **B.** CARP3-smFLAG (TcCLB.506681.40), and **C.** hypothetical protein-FLAG (TcCLB.510329.180). DNA ladder shown with sizes (bp) on left.